Computational Structure Design of a Bio-Inspired Armwing Mechanism

Eric Sihite, Peter Kelly, and Alireza Ramezani

***Abstract*—Bat membranous wings possess unique functions that make them a good example to take inspiration from and transform current aerial drones. In contrast with other flying vertebrates, bats have an extremely articulated musculoskeletal system which is key to their energetic efficiency with impressively adaptive and multimodal locomotion. Biomimicry of this flight apparatus is a significant engineering ordeal and we seek to achieve mechanical intelligence through sophisticated interactions of morphology. Such morphological computation or mechanical intelligence draws our attention to the obvious fact that there is a common interconnection between the boundaries of morphology and closed-loop feedback. In this work, we demonstrate that several biologically meaningful degrees of freedom can be interconnected to one another by mechanical intelligence and, as a result, the responsibility of feedback-driven components (e.g., actuated joints) is subsumed under computational morphology. The results reported in this work significantly contribute to the design of bio-inspired Micro Aerial Vehicles (MAVs) with articulated body and attributes such as efficiency, safety, and collision-tolerance.**

***Index Terms*—Biomimetics, soft robot materials and design, mechanism design.**

I. Introduction

THE overall goal of this work is to advance the theory and practice of aerial robots that are soft, agile, collision-tolerant, and energetically efficient by the biomimicry of key airborne vertebrate flight characteristics. In recent years, much attention has been drawn to make our residential and work spaces smarter and to materialize the concept of smart cities [1]. As a result, safety and security aspects are gaining ever growing importance [2] and drive a lucrative market. Systems that can provide situational awareness to humans in residential and work spaces or contribute to dynamic traffic control in cities will result in large-scale intelligent systems with enormous societal impact and economic benefit.

Current state-of-the-art solutions with rotary or fixed-wing features fall short in addressing the challenges and pose extreme dangers to humans. Fixed or rotary-wing systems are widely applied for surveillance and reconnaissance, and there is a growing interest to add suites of on-board sensors to these unmanned aerial systems (UAS) and use their aerial mobility to monitor and detect hazardous situations in residential spaces. While, these systems, e.g., quadrotors, can demonstrate agile maneuvers and have demonstrated impressive fault-tolerance in aggressive environments, quadrotors and other rotorcrafts require a safe and collision-free task space for operation since they are not collision-tolerant due to their rigid body structures. The incorporation of soft and flexible materials into the design of such systems has become common in recent years, yet, the demands for aerodynamic efficiency prohibit the use of rotor blades or propellers made of extremely flexible materials.

The flight apparatus of birds and bats can offer invaluable insights into novel micro aerial vehicle (MAV) designs that can safely operate within residential spaces. The pronounced body articulation (morphing ability) of these flyers is key to their unparalleled capabilities. These animals can reduce the wing area during upstrokes and can extend it during downstrokes to maximize positive lift generation [3]. It is known that some species of bats can use differential inertial forces to perform agile zero-angular momentum turns [4]. Biological studies suggest that the articulated musculoskeletal system of animals can absorb impact forces therefore can enhance their survivability in the event of a collision [5].

The objective of this letter is to design and develop a bio-inspired soft and articulated armwing structure which will be an integral component of a morphing aerial co-bot. In our design, we draw inspiration from bats. Bat membranous wings possess unique functions [6] that make them a good example to take inspiration from and transform current aerial drones. In contrast with other flying vertebrates, bats have an extremely articulated musculoskeletal system, key to their body impact-survivability and deliver an impressively adaptive and multimodal locomotion behavior [7]. Bats exclusively use this capability with structural flexibility to generate the controlled force distribution on each wing membrane. The wing flexibility, complex wing kinematics, and fast muscle actuation allow these creatures to change the body configuration within a few tens of milliseconds. These characteristics are crucial to the unrivaled agility of bats [8] and copying them can potentially transform the state-of-the-art aerial drone design.

A. State-of-the-Art Morphing Wing Designs

An untethered, self-sustained, and autonomous robotic platform that can mimic bird and bat explosive wing articulations is

Manuscript received February 24, 2020; accepted June 16, 2020. Date of publication July 17, 2020; date of current version July 30, 2020. This work was supported by the NRI: EAGER: Teaching Aerial Robots to Perch Like a Bat via AI-Guided Design and Control (NSF-IIS 1944964; Oct, 2019–Sep, 2020; $102,367.00). This letter was recommended for publication by Associate Editor X. Liu and Editor X. Wu upon evaluation of the Reviewers' comments. *(Corresponding author: Alireza Ramezani.)*

The authors are with the SiliconSynapse Laboratory, Department of Electrical and Computer Engineering, Northeastern University, Boston, MA 02119 USA (e-mail: ericsihite@gmail.com; kelly.pe@husky.neu.edu; a.ramezani@northeastern.edu).

This letter has supplementary downloadable material available at http://ieeexplore.ieee.org provided by the authors.

Digital Object Identifier 10.1109/LRA.2020.3010217

a significant design problem after noting the prohibitive design restrictions such as payload, size, power, etc. MAVs with morphing body [9]–[11] have distinguished themselves from other archetypal MAVs through their superior performance. However, unlike a wide variety of conventional flapping wing robots that have been developed in various sizes, ranging from insect-style flapping MAVs [12] to larger bird-style robots [13]–[16], these morphing designs are not well explored.

The wings of flapping MAVs are commonly made of a single wing segment and are articulated to either flapping about a constant axis of rotation [17], [18], or about a rotating axis which has the effect of adjusting the wing's angle of attack [19], [20]. In these designs, wing folding is overlooked. The supination-pronation motion that allows the wing to produce lift during upstrokes is achieved either passively or to a limited degree not comparable to its biological counterparts.

The importance of wing folding in animal flight has motivated recent designs [20]. However, the prohibitive design challenges have set limits in copying the pronounced mediolateral or flexion-extension movements found in animals flight apparatus. *SmartBird* [20] wings have two wing segments and they bend at the elbow joint to expand and retract the wings during downstrokes and upstrokes, respectively. These movements maximize the positive lift generation.

Other works [21]–[24] attempted to design armwing retraction mechanisms and used the opportunity to study the underlying control mechanisms [25]–[29] based on which bats perform sharp banking turns and diving maneuvers. The morphing wing design introduced by [23] considered substantially fewer joints in an un-tethered system by erecting a *kinetic sculpture* that embodied several biologically meaningful modes from bats. Contrary to [23], many string-and-pulley-activated joints were incorporated in the morphing wings introduced by [30] and [31] that allowed a greater control authority over independent joint movements. However, these designs were tethered.

All of these morphing wings have achieved great success in copying kinematics and dimensional complexity of bat flight apparatus. However, the armwing mechanisms present in these robots were not capable of copying the dynamically versatile wing conformations found in bats.

B. A Design Philosophy Based on Coalescing Mechanical Intelligence and Closed-Loop Feedback

The emerging ideas surrounding achieving computation in robots through sophisticated interactions of morphology, however, has begun to change motion design and control in robots that have prohibitive design restrictions. Such a computation, called *morphological computation* or *mechanical intelligence* [32], draws our attention to the obvious fact that there is a common interconnection – and in some morphologies these couplings are very tight – between the boundaries of morphology and closed-loop feedback.

Controllers lie in the space of abstract computation, and are usually implemented in computational layers or are programmed into the system. However, if mechanical interactions can also perform computation, it becomes possible for the morphology to play a role of computation in the system, and in effect part of the role of the controller is subsumed under computational morphology. As a result, a cleverly designed structure can facilitate control requirements by performing part of the computation. These natural and biologically motivated computational structures can be very favorable in morphing MAV design and have been overlooked because of sophistication associated with design and fabrication. Particularly, we will explore such design approaches to copy dynamically versatile wing conformations of bats flight apparatus.

This work extends our prior contributions [21]–[24] by offering kinetic sculpture designs that can capture bat dynamically versatile wing conformations. These structures consist of rigid and flexible materials that are monolithically fabricated using novel computed-aided fabrication methods and additive manufacturing technology (PolyJet 3D printing). Like its predecessor, this armwing structure articulation is also designed to expand and retract within a single wingbeat through a series of crank and four-bar mechanisms as it is actuated by a single brushless DC motor. The use of a monolithic rigid and flexible armwing structure in a flying robot is novel and might be very impactful for flapping robot design as this structure is capable of mimicking the range of motion and flexibility of an actual bat armwing. This mechanism design assumes a planar flapping motion and only articulates the wing plunging and extension-retraction gaits. The addition of other modes such as supination-pronation, sweeping motion, and 3D flapping gait will be considered in our future work.

This letter is outlined as follows: (1) the armwing mechanical design which outlines the wing structure, mechanism, and hinge design in great detail, (2) wing conformation kinematics and design optimization to follow a specified trajectory, (3) structural and sensivity analysis of the optimized wing design, and (4) future work and conclusions.

II. Mechanical Design

In order to successfully develop a robotic wing structure that can mimic the speed and flexibility of a natural bat wing, we must work to achieve a set of design criterion: (a) a mechanical structure that mimics as many meaningful degrees-of-freedom (DoF) as possible from the natural bat wing, (b) a robust and flexible wing structure which facilitates control through morphological computation, and (c) a small, lightweight, and compact mechanism. The meaningful DoFs we considered in this letter are the plunging motion along with the wing extension/retraction, where the control is facilitated by either changing the wing morphology or by directly articulating the armwing kinetic sculpture.

A bat wing has up to 34 DoF and unparalleled flexibility [30] which is not feasible to replicate using a rigid mechanical structure in a small and compact form factor. By using flexible joints to form a compliant structure, we can mimic some of the natural bat wing's flexibility and the important DoFs for flapping flight packaged in a very compact mechanical structure. The multi-material printing capability of PolyJet 3D printers allows

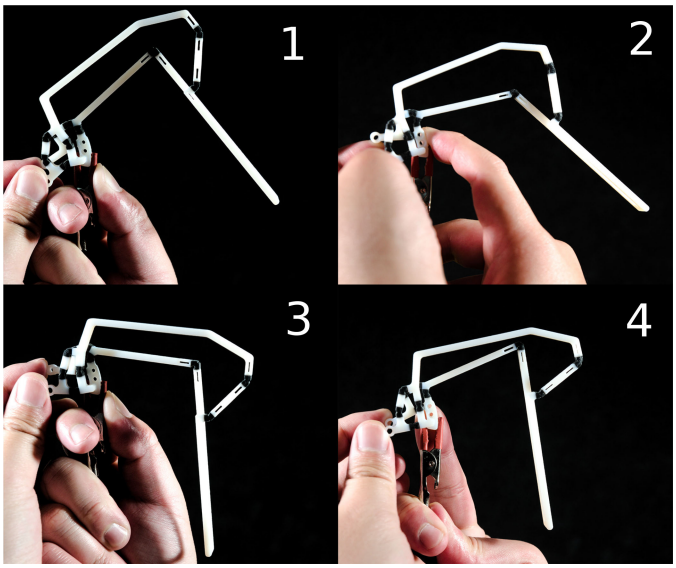

Fig. 1. The time-lapsed images of the bat armwing articulation. Images 1–2 show the wing downstroke/expansion motion while images 3–4 show the wing upstroke/retraction motion. The armwing is monolithically fabricated using both rigid and flexible materials in a PolyJet 3D printer.

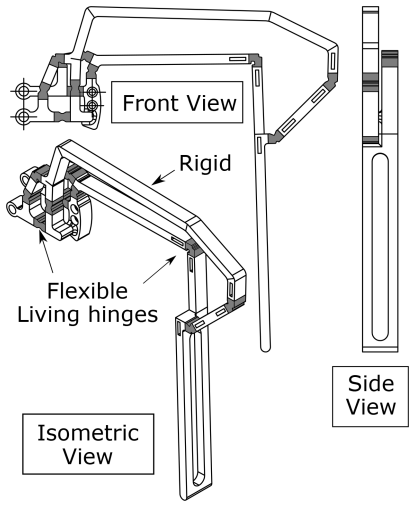

Fig. 2. The CAD model of the monolithic wing structure for PolyJet 3D printing. The white and greyed sections are rigid and flexible hinges respectively which are made using a mixture between the rigid *Vero White* and the flexible *Agilus Black*.

us to fabricate a monolithic wing structure composed of rigid and flexible materials which is shown in Fig. 2.

The wing structure is articulated using a series of cranks and four-bar linkage mechanisms. This mechanism is actuated with only a single motor, therefore the wing expansion/retraction is a slave to the flapping motion as it is actively actuated by the motor. In order to achieve a small and lightweight structure, we constrain our design such that the driving mechanism is contained in a capsule-shaped tube of 50 mm diameter and 75 mm long. The total wingspan of the robot is approximately 300 mm wide which follows a similar form factor as our previous work [23], and we aim for a robot that weighs approximately 20 grams.

TABLE I
TABLE OF THE TESTED HINGE MATERIALS

Material	Shore Hardness (A)	Elongation at Break (%)
FLX 9850	50 - 55	170 - 210
FLX 9870	60 - 70	120 - 140
FLX 9885	80 - 85	70 - 90

A. Flexible Hinge Design

The flexible joints are the core component of the wing's compliant mechanism and there are several design considerations that can be made which affect the hinge stiffness and robustness. There are several design variations for a compliant joint as outlined in [33], where they vary in size, off-axis stiffness, axis drift, stress concentration, and range of motion. In order to satisfy our design target of a small and lightweight aerial robot, we choose to use the simple planar notch design as shown in Fig. 2. This notch design has a disadvantage in the form of very low off-axis stiffness, particularly the torsional stiffness. The PolyJet flexible materials, in the case of Stratasys PolyJet 3D printers, come in Shore hardness scale range of 30 A to 85 A which is formed by mixing the rigid *Vero White* and the flexible *Agilus Black* [34]. A softer and more flexible material has better compliance which means that it can safely deform to counteract unexpected forces. However, it will also has worse resistance to torsion and off-axis perturbations.

The planar four-bar linkage mechanism in Fig. 2 assumes that the structure does not deform in the off-plane directions, so the low off-axis stiffness can be a significant issue. This problem can be addressed by using a larger cross-sectional area or by reinforcing the hinge with a flexible support structure post-fabrication to increase the off-axis stiffness of the hinge. The larger cross-sectional area increases the durability of the hinge but also increase the overall hinge stiffness and weight which is a design trade-off.

For our wing prototypes, we choose a combination of 1.3 mm and 2 mm hinge thickness with the flexible materials shown in Table I, where the material property values are taken from [34]. We use a shaft thickness of 3 mm and depth of 5 mm in all of our link design. The deep shaft design increases the off-axis stiffness of the armwing structure and the durability of the hinge. The three material hardness in Table I capture a wide range of stiffness which can be a great reference point for our future design iterations. Each armwing prototypes we fabricated has the same hinge thickness and material within an individual wing. Conversely, it is possible to use varying hinge design and properties depending on each joint's stress and flexibility requirements which we can investigate in our future work.

B. Driving Mechanism Design

The armwing driving mechanism can be separated into two sets of crank and four-bar mechanisms, as shown in Fig. 3, where they articulate the linkages representing the humerus and radius bones in a bat's arm. Both crank mechanisms operate at the same frequency but with a different phase $\Delta\phi$ which articulates the desired wing extension and retraction during a specific timing

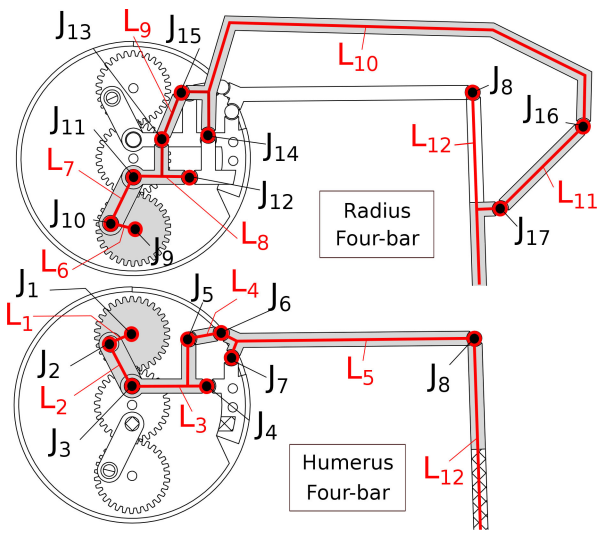

Fig. 3. The links and hinges present in the wing linkage mechanism, which is composed of 12 links ($L_i, i \in \{1, \ldots, 12\}$) and 17 joints/living hinges ($J_k, k \in \{1, \ldots, 17\}$). The crank mechanisms drive links L_3 and L_8 which actuate the shoulder and elbow joints (J_7 and J_8) respectively.

within a wingbeat. The monolithic wing structure has 8 links and 11 hinges per wing while the gears and crank mechanism add 4 links and 6 revolute joints per wing, which results in a grand total of 12 links and 17 joints per wing. The mechanism is designed by assuming that the flexible hinges act like an ideal axial joint which follows the parallel linkage mechanism design principles.

The humerus and radius links have a length of 50 mm and 90 mm respectively, which is based on the conformation of the *Rousettus aegyptiacus* [35]. This bat flies under a flapping rate of approximately 10 Hz which we will also try to emulate. Due to the space constraints, the four-bar mechanisms are placed off-plane and parallel from each other. The gears which drive the four-bar mechanisms must be placed in the midpoint of the body so that we can implement a symmetric wing assembly. This way, each side of the wing can utilize the same wing structure and the mechanisms can be connected using a spur gear or other means of power transmission. This configuration results in a horizontally-symmetric but off-plane wing skeletal structure. However, this should not be a major issue because the wing membranes can be attached in a symmetric fashion.

C. Monolithically Fabricated Bat Armwing Structure

The 3D printed monolithic bat armwing structure, which weighs 7 grams, can be seen in Fig. 1 as it is being articulated from the crank arms. This flexible armwing conformation is capable of achieving the desired wing expansion and retraction. We tested several combinations of hinge thickness and materials as listed in Table I. As expected, there is a large variation in the stiffness and ease of articulation for each wing variant. We found out that the armwing with durometer scale of 50 A is simply too soft to be used in the wing articulation and it has very little off-plane and torsional stiffness even in the thicker hinge design. The armwing with the durometer scale of 85 A and 2 mm hinge thickness is too stiff and relatively brittle. However, the wing with 85 A durometer and 1.3 mm hinge thickness has excellent off-plane and torsional stiffness which can be beneficial as long as we can provide the torque to actuate the stiff armwing. In the end, we conclude that the wings with 1.3 mm hinge thickness and either 70 A or 85 A durometer have the best overall result in the wing articulation and stiffness.

TABLE II
OPTIMIZED WING CONFORMATION DESIGN PARAMETERS ($\boldsymbol{q}$)

Param.	Value	Param.	Value	Param.	Value
l_1	3.88 mm	l_9	9.01 mm	p_{4y}	2.90 mm
l_2	11.5 mm	l_{10a}	5.00 mm	p_{7x}	17.5 mm
l_{3a}	14.7 mm	l_{10b}	7.00 mm	p_{7y}	10.4 mm
l_{3b}	6.91 mm	l_{10c}	70.0 mm	p^*_{9x}	0 mm
l_{3c}	11.0 mm	l_{10d}	9.40 mm	p^*_{9y}	-15 mm
l_4	9.46 mm	l_{11}	25.1 mm	p^*_{12x}	$= l_{8a}$
l_{5a}	3.35 mm	l_{12a}	30.0 mm	p_{12y}	-5.00 mm
l_{5b}	4.56 mm	l_{12b}	9.98 mm	p_{14x}	15.8 mm
l_6	3.46 mm	l^*_h	50 mm	p_{14y}	4.68 mm
l_7	12.0 mm	l^*_r	90 mm	α_5	31.0°
l_{8a}	10.0 mm	p^*_{1x}	0 mm	ϕ_0	1°
l_{8b}	7.00 mm	p^*_{1y}	15 mm	$\Delta\phi$	18.2°
l_{8c}	10.00 mm	p^*_{4x}	$= l_{3a}$		

Note: parameters with superscript * has a constrained value.

The mechanism shown in Fig. 3 was developed by simulating the rigid body linkages in Solidworks Motion Study. This methodology is suffice to discover the initial configuration that works decently well. However, in order to get the best result, we must use a design optimization framework to search for the best armwing conformation which follows the desired wing gait we specified.

III. WING CONFORMATION DESIGN OPTIMIZATION

The wing mechanism is composed of rigid links and flexible hinges which can be modeled as rigid body linkages with linear and rotational stiffness at the joints, as outlined in [36]. However, fully modeling the flexible joints is very difficult considering the complexity of our design. Therefore, we designed the mechanism and performed our analysis assuming a rigid parallel linkage mechanism. This section outlines the rigid body kinematic formulation and the wing morphology optimization problem to follow a specific flapping trajectory.

A. Kinematic Formulation

Assuming rigid body kinematics, the armwing mechanism has two DoF per wing which are represented by the two crank arms of the wing (links 3 and 8). Since the crank gears are coupled, the assembled wing mechanism only has one DoF which means that the full system states can be solved from the driving gear angle if the value is known.

Referring to Fig. 3, let θ_i be the angle of joint i with respect to the horizontal axis and $\boldsymbol{p}_i = [p_{ix}, p_{iy}]^T$ be the position of joint i. Table II lists the wing design parameters ($\boldsymbol{q}$), where l_j represents the length components of link L_j. The dimension parameters for non-straight links are shown in Fig. 4. The actuation phase difference $\Delta\phi$ defines the relation between two

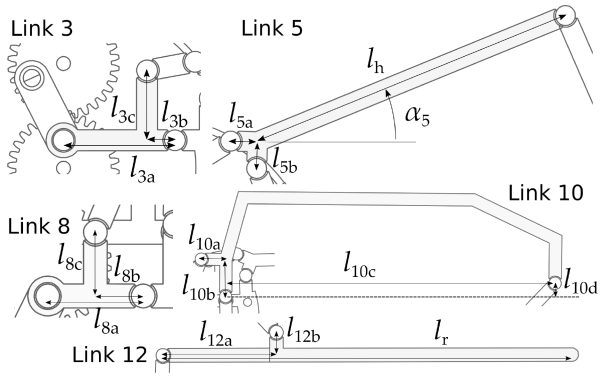

Fig. 4. The dimensions of the links that are not a simple straight link. All of the length parameters except of l_h and α_5 are setup perpendicularly or parallel to each others.

crank gear angles $\theta_1 = \omega t + \phi_0$ and $\theta_9 = \theta_1 + \Delta\phi$, where ω is the flapping frequency.

Given the humerus mechanism driving gear angle θ_1, the system states can be solved sequentially as follows:

1) *Solve the humerus mechanism:* Given θ_1, solve the four-bar linkages (J_1, J_2, J_3, J_4) for $\boldsymbol{p}_5(\theta_4)$, then solve the next four-bar linkages (J_4, J_5, J_6, J_7) for $\boldsymbol{p}_8(\theta_7)$.
2) *Solve the radius mechanism:* Calculate $\theta_9 = \theta_1 + \Delta\phi$, then solve for the four-bar linkages (J_9, J_{10}, J_{11}, J_{12}) for $\boldsymbol{p}_{13}(\theta_{12})$, then solve the next four-bar linkages (J_{12}, J_{13}, J_{15}, J_{14}) for $\boldsymbol{p}_{16}(\theta_{14})$. Finally, solve the last three-bar linkage (J_8, J_{16}, J_{17}) for $\boldsymbol{p}_{17}(\theta_8)$.

The four-bar and three-bar linkages listed above can be solved by using a root-finding algorithm. For example, given θ_1, the solution to the four-bar linkages (J_1, J_2, J_3, J_4) can be found by solving the constraint equation

$$h_c(\theta_4) = |\boldsymbol{p}_2(\theta_1) - \boldsymbol{p}_3(\theta_4)| - l_2 = 0$$

$$\boldsymbol{p}_2(\theta_1) = l_1 \begin{bmatrix}\cos(\theta_1)\\ \sin(\theta_1)\end{bmatrix}, \quad \boldsymbol{p}_3(\theta_4) = -l_{3a} \begin{bmatrix}\cos(\theta_4)\\ \sin(\theta_4)\end{bmatrix}, \quad (1)$$

for θ_4 which can be used to calculate $\boldsymbol{p}_5(\theta_4)$. The remaining linkages can be solved in a similar fashion.

The angles that are biologically meaningful in this wing articulation is the shoulder and elbow angles, θ_s and θ_e respectively, where θ_s represents the upstroke/downstroke motion and θ_e represents the retraction/expansion motion. We can then formulate a solver equation such that given the wing design parameters and the drive gear angle $\theta_1 \in [0, 2\pi] + \phi_0$, solve for θ_s and θ_e

$$\theta_s = \theta_7 + \alpha_5, \qquad \theta_e = \theta_8 - \theta_s + \pi$$

$$\theta_s, \theta_e^\top = \boldsymbol{f}_m(\boldsymbol{q}, \theta_1). \quad (2)$$

Note that the solution of θ_e depends on θ_s but not the other way around.

B. Design Optimization

The ideal flapping motion that we are looking for has the following properties: (1) the wing extends and retracts during downstroke and upstroke respectively, (2) the wing is already partially expanded before the downstroke motion begins. The desired trajectories $\hat{\theta}_s$ and $\hat{\theta}_e$ can be seen in Fig. 5 (b) , which are defined as the following sinusoidal functions

$$\hat{\theta}_s = 35^\circ \sin(\phi) - 10^\circ$$

$$\hat{\theta}_e = -0.5 \tan^{-1}\left(\frac{-0.5\sin(\phi+2\pi/3)}{1+0.5\cos(\phi+2\pi/3)}\right) 45^\circ + 120^\circ, \quad (3)$$

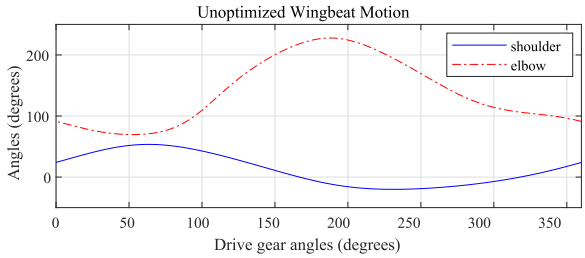

(a) Unoptimized armwing angles.

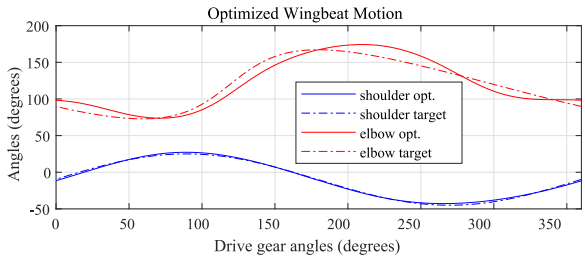

(b) Optimized armwing angles and their target trajectories.

Fig. 5. The unoptimized and optimized armwing shoulder and elbow angles within a single wingbeat. The optimization has successfully found the parameters that results in close tracking to the target trajectory.

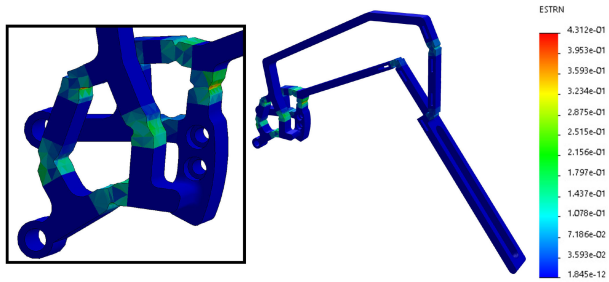

(a) Wing expansion before the downstroke.

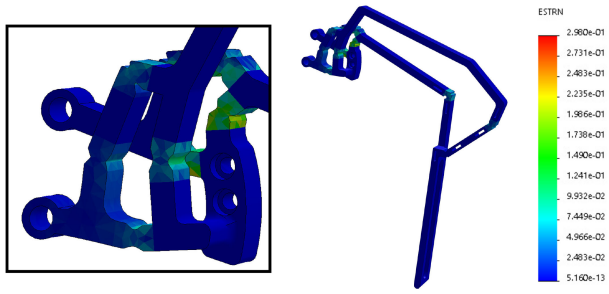

(b) Wing retraction before the upstroke.

Fig. 6. FEA of the compliant mechanism under static torques acting on the crank arms. The strain values are shown at the right side.

where $\phi \in [0, 2\pi)$. $\hat{\theta}_e$ is a skewed sinusoidal function which allows the wing to expands faster than the retraction and have a full wingspan in the middle of the downstroke.

The design optimization will solve for some of the mechanism design parameters $\boldsymbol{q}$ which is listed in Table II, using our initial mechanism design in Solidworks for the initial $\boldsymbol{q}$. There are 38 parameters in the design space of this armwing and we constrain some of these parameters to fit our design criterion and reduce the search space of the optimizer. In order to have a symmetric gait between the left and right wing, the drive gears must be centered ($p_{1x} = p_{9x} = 0$) and the crank arm maximum horizontal length must be aligned with the body y axis ($p_{4x} = l_{3a}$, $p_{12x} = l_{8a}$). Additionally, we fix the values for the following parameters: $p_{1y} = 15$ mm, $p_{9y} = -15$ mm, $l_h = 50$ mm, and $l_r = 90$ mm. This leaves us with 30 design parameters to optimize.

Considering the large design space of this wing structure, solving for all 30 parameters at the same time is not practical due to the large computational time and search space. The radius mechanism must follow a trajectory in relation to the humerus mechanism to articulate the appropriate elbow angle. Therefore, we can separately optimize the humerus and radius mechanisms, starting from the humerus mechanism. The humerus and radius mechanisms have 13 and 17 design parameters, respectively.

The optimization problem can be formulated as

$$\begin{aligned} \min_{\boldsymbol{q}} \quad & (\boldsymbol{y}^T \boldsymbol{y})/N \\ \text{subject to:} \quad & \boldsymbol{q}_{\min} \leq \boldsymbol{q} \leq \boldsymbol{q}_{\max}, \quad \boldsymbol{f}_c \leq 0, \end{aligned} \tag{4}$$

where the the cost function is the mean squared value of $\boldsymbol{y}$ which is the difference between target vs. the simulated trajectory, N is the data size, $\boldsymbol{q}$ is the parameter to optimize, $\boldsymbol{q}_{\min}$ and $\boldsymbol{q}_{\max}$ are the parameter bounds, and $\boldsymbol{f}_c$ is the constraint function. We used the interior-point method as the optimization algorithm in Matlab which has successfully found a solution that matches the target trajectory well.

1) Humerus Mechanism Optimization: The humerus mechanism is optimized using the cost function $\boldsymbol{y} = \hat{\boldsymbol{\theta}}_s - \boldsymbol{\theta}_s$ where $\boldsymbol{\theta}_s$ is the trajectory vector gained by solving (2) for $\theta_{s,k}$ given the input angle $\theta_{1,k} = 2\pi k/N + \phi_0$, $k = \{1, \ldots, N\}$. We then optimize the following 13 parameters

$$\begin{aligned} \boldsymbol{q}_H = [&l_1, l_2, l_{3a}, l_{3b}, l_{3c}, l_4, l_{5a}, l_{5b}, \\ &\alpha_5, p_{4y}, p_{7x}, p_{7y}, \phi_0], \end{aligned} \tag{5}$$

subject to the following constraints: (1) the body-fixed joint positions ($\boldsymbol{p}_4$ and $\boldsymbol{p}_7$) are within the the robot's 50 mm diameter cylindrical body, (2) the linkages don't intersect or block each other, and (3) the length constraints for the linkages to prevent singularity in the four-bar mechanism. For example, the constraint equation $(l_1 + |\boldsymbol{p}_4 - \boldsymbol{p}_1|) - 0.8\,(l_2 + l_{3a}) < 0$ constrains the linkage lengths to prevent singularity in the four-bar mechanism (J_1, J_2, J_3, J_4). We use a similar constraint for the other four-bar mechanisms.

2) Radius Mechanism Optimization: Once the humerus parameters has been optimized, we can then optimize the remaining 17 parameters for the radius mechanism

$$\begin{aligned} \boldsymbol{q}_R = [&l_6, l_7, l_{8a}, l_{8b}, l_{8c}, l_9, l_{10a}, l_{10b}, l_{10c}, \\ &l_{10}\,d, l_{11}, l_{12a}, l_{12b}, p_{12y}, p_{14x}, p_{14y}, \Delta\phi], \end{aligned} \tag{6}$$

subject to similar constraints and follow the same procedures as the humerus optimization problem. The cost function calculates the trajectory error $\boldsymbol{y} = \hat{\boldsymbol{\theta}}_e - \boldsymbol{\theta}_e$.

C. Optimization Results and Discussion

Fig. 5 shows the simulation of the shoulder and elbow angles for one flapping cycle using the rigid body kinematic formulation shown in (2). The unoptimized design trajectories, shown in Fig. 5 (a), has a range of $\theta_s \in [-20^\circ, 54^\circ]$ and $\theta_e \in [70^\circ, 228^\circ]$ which have the characteristics of the ideal flapping motion that is discussed in Section III-B. However, the maximum elbow angle of 228° raises some concerns since that indicates a nontrivial joint hyperextension which might have an adverse effect on the armwing structure.

The design optimization has successfully found the design parameters $\boldsymbol{q}$ shown in Table II, which have 15.8% average difference compared to the initial values and closely follow the target trajectories as shown in Fig. 5 (b), with R^2 values of 0.997 and 0.920 for θ_s and θ_e respectively which indicate a good fit. The optimized trajectory has motion range of $\theta_s \in [-43^\circ, 27^\circ]$ and elbow angle range of $\theta_e, \in [74^\circ, 174^\circ]$ which does not have the joint hyperextension present in the unoptimized design. The elbow joint and wingtip trajectories of the optimized design can be seen in Fig. 7. We also need to make sure that there is no extreme hinge bending angles compared to its resting position to avoid breakage. Joints 8, 16, and 17 which are all connected to the radius link L_{12} have a maximum bending angles of 80° to 90° that bend significantly more towards one side than the other. Joint 11 has a maximum bending angle of 65° while the other joints have the maximum bending angle of less than 45°.

IV. Structural and Sensitivity Analysis

This section discusses the structural and sensitivity analysis done on the optimized armwing structure. The structural analysis is done by using Solidworks Simulation FEA to simulate the flexible material bending as the armwing is articulated. Then a sensitivity analysis is done to show which design parameters have the most impact to the flapping gait and how the trajectories change with these parameters.

A. Structural Analysis

Fig. 6 shows the strain of the armwing structure during some of the key moments which is simulated using the Solidworks Simulation FEA under static torques acting on the crank arms. We use the material property of FLX9870 (Table I) which has the density of 1.15 g/cm^3 and average tensile strength of 5 MPa [34]. The simulation is done with the hyperelastic Mooney-Rivlin model using the material constants of a rubber shown in [37], with a Poisson's ratio of 0.4999, and first and second material

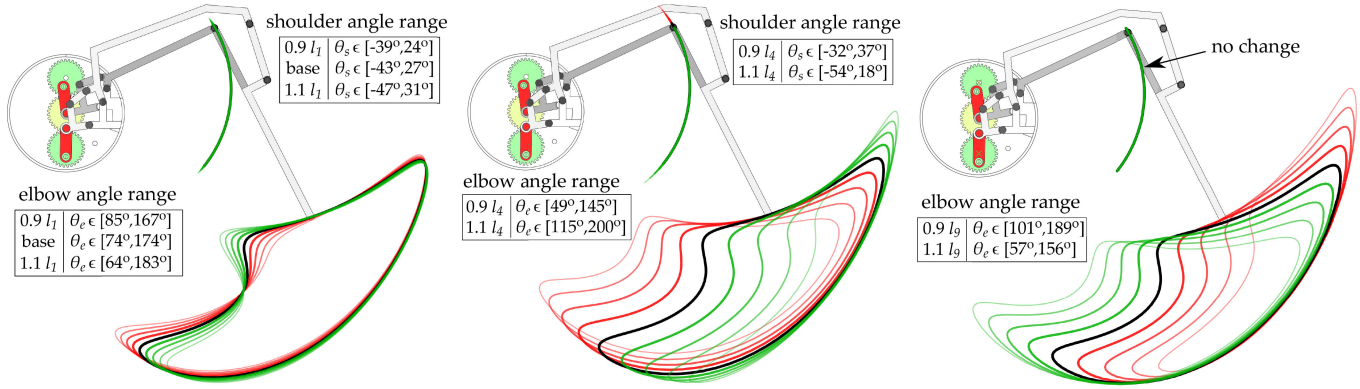

(a) Adjustment to l_1 length. (b) Adjustment to l_4 length. (c) Adjustment to l_9 length.

Fig. 7. Armwing elbow joint and wingtip trajectories generated by varying one of the design parameter. The parameter is varied between 90% and 110% of the optimal value listed in Table II. The green and red trajectory colors indicate larger and smaller parameter values respectively.

constants of 0.3339 Mpa and -0.337 kPa respectively. The key moments we considered are the beginning of the downstroke and upstroke motion where the mechanism starts to change its direction. As shown in Fig. 6, the maximum strain during these two motions are 43% and 30% respectively. Since FLX9870 has an elongation at break of 120–140%, we have an adequate margin to deal with unforeseen strains which might arise due to unexpected torsional and off-plane perturbations. A different hinge design can be considered to further reduce the stress/strain concentration, but our space constraints significantly limit our design options.

B. Sensitivity Analysis

The sensitivity analysis is done to determine how much the parameters in $\boldsymbol{q}$ affect the θ_s and θ_e trajectories. Let A and M be the peak-to-peak amplitude and mean of the joint trajectories respectively, and $\Delta\theta$ be the phase difference between the peaks of θ_s and θ_e. The rate of change of A_e, A_s, M_e, M_e, and $\Delta\theta$ are evaluated about the optimized parameters $\boldsymbol{q}$ listed in Table II.

Table III shows the Jacobian of the A, M, and $\Delta\theta$ vs $\boldsymbol{q}_H$ and $\boldsymbol{q}_R$. The parameters have the following units: mm for lengths and positions, and rad for the angles. The most sensitive parameter is l_1 which affects the amplitudes A_s and A_e the most, and also significantly affects $\Delta\theta$ as well. The shoulder mean trajectory M_s are mostly affected by l_4, l_{3a}, l_{3b}, l_2, and p_{7x}. The elbow trajectory is mostly affected by the parameters l_6 and l_7. The angle parameters α_5 significantly affects M_s, M_e, and A_e while $\Delta\phi$ affects A_e, but they have a different unit than the length parameters so it is difficult to directly compare their effects. In conclusion, the length parameters of the links closer to the driving gears are among the most sensitive parameters in our mechanism.

Fig. 7 shows how the elbow joint and wingtip trajectory varies with some of the design parameters, particularly l_1, l_4, and l_9. l_1 is chosen as it is the most sensitive parameter in the design while l_4 and l_9 are simple links that are relatively sensitive to change in the shoulder and elbow joint angle trajectories. l_4 and l_9 are also chosen to promote our control framework where we adjust the flapping gait by changing the wing conformation. These links are simple straight links and we might be able change the design to support variable length linkages on these links. The mechanism design and implementation of this idea can be a part of our future work. The values tested in Fig. 7 are adjusted by $\pm 2.5\%$, up to $\pm 10\%$ from their original values in Table II. The green and red lines represent an increase and decrease compared to the original parameter value respectively. As shown in Fig. 7 (c), the elbow joint trajectory is unaffected by a change in l_9 which is also shown in Table III. This indicates that we can adjust θ_e independently from θ_s which supports our idea of applying control through morphology manipulation.

TABLE III
SENSITIVITY ANALYSIS OF THE WING MECHANISM PARAMETERS

$\boldsymbol{q}$	A_s	A_e	M_s	M_e	$\Delta\theta$
l_1	**19.7**	**47.7**	-1.40	-3.47	**18.6**
l_2	-2.79	2.48	9.86	-28.6	-4.71
l_{3a}	-2.94	-17.7	-10.2	30.9	-1.23
l_{3b}	-1.51	8.85	11.1	**-30.97**	-5.21
l_{3c}	1.87	2.93	-2.06	5.74	0
l_4	1.83	-8.14	**-11.3**	31.6	3.81
l_{5a}	-5.49	-19.8	-6.83	22.5	-5.37
l_{5b}	-7.47	-6.59	7.79	-21.5	-7.89
α_5	0	68.5	57.3	-163	0
p_{4y}	-6.96	-6.22	8.56	-21.4226	-12.4
p_{7x}	-2.36	7.40	11.0	-30.3708	-6.19
p_{7y}	4.22	11.3	1.28	-9.05	5.18
ϕ_0	$-2.2\cdot10^{-4}$	$-2.3\cdot10^{-4}$	$-4.3\cdot10^{-4}$	$-2.5\cdot10^{-4}$	0
l_6	0	**-23.7**	0	14.2	**-20.8**
l_7	0	8.69	0	**-24.9**	1.5
l_{8a}	0	12.3	0	-15.0	5.4
l_{8b}	0	-9.5	0	15.0	-5.14
l_{8c}	0	-1.14	0	-14.0	-5.4
l_9	0	6.07	0	-20.9	-2.0
l_{10a}	0	10.8	0	-16.5	7.2
l_{10b}	0	4.36	0	11.7	7.71
l_{10c}	0	-2.37	0	0.045	0.514
l_{10d}	0	-1.08	0	2.5	0
l_{11}	0	1.01	0	-2.77	0
l_{12a}	0	-1.3	0	2.51	0
l_{12b}	0	-0.434	0	-1.08	0
p_{12y}	0	-6.09	0	10.6	-3.6
p_{14x}	0	-6.51	0	15.5	2.28
p_{14y}	0	-4.28	0	16.3	0
$\Delta\phi$	0	117.0	0	12.1	0

Note: units are rad/mm for length or position and rad/rad for angles.

V. Conclusion and Future Work

We present a novel bio-inspired monolithic bat armwing structure with both flexible and rigid materials. This armwing structure is designed to expand and retract during the wing flapping motion to maximize the net lift produced by the wing. The design optimization along with the structural and sensitivity analysis have also been presented in this letter, where a design optimized wing conformation has been successfully found and analyzed.

In the future work, we will propose a design revision for the armwing structure based on the design optimization framework and the appropriate flexible hinge design. Then we will develop the complete bat-robot with both sides of the wings fully actuated and also investigate the control algorithms that can achieve stable flight, either by adjusting the wing conformation or through different means of actuation. The compliant structure can also be augmented to articulate a 3D flapping gait which captures supination-pronation and sweeping motion. Other PolyJet 3D printer fabrication options can also be investigated, such as embedding material in the 3D printed structure [38]. This might open up a new possibilities in our armwing design that can save space and also reduce weight in our robot mechanical assembly.

References

[1] J. Everaerts *et al.*, "The use of unmanned aerial vehicles (UAVs) for remote sensing and mapping," *Int. Arch. Photogrammetry, Remote Sens. Spatial Inf. Sci.*, vol. 37, no. 2008, pp. 1187–1192, 2008.

[2] I. Pavlidis, V. Morellas, P. Tsiamyrtzis, and S. Harp, "Urban surveillance systems: From the laboratory to the commercial world," *Proc. IEEE*, vol. 89, no. 10, pp. 1478–1497, Oct. 2001.

[3] B. W. Tobalske, "Biomechanics and physiology of gait selection in flying birds," *Physio Biochem. Zoology*, vol. 73, no. 6, pp. 736–750, 2000.

[4] D. K. Riskin, A. Bergou, K. S. Breuer, and S. M. Swartz, "Upstroke wing flexion and the inertial cost of bat flight," *Proc. Roy. Soc. B: Biol. Sci.*, vol. 279, no. 1740, pp. 2945–2950, 2012.

[5] T. J. Roberts and N. Konow, "How tendons buffer energy dissipation by muscle," *Exercise Sport Sci. Rev.*, vol. 41, no. 4, pp. 186–193, 2013.

[6] H. Tanaka, H. Okada, Y. Shimasue, and H. Liu, "Flexible flapping wings with self-organized microwrinkles," *Bioinspiration Biomimetics*, vol. 10, no. 4, 2015, Art. no. 046005.

[7] D. K. Riskin *et al.*, "Quantifying the complexity of bat wing kinematics," *J. Theor. Biol.*, vol. 254, no. 3, pp. 604–615, 2008.

[8] A. Azuma, "The biokinetics of flying and swimming," *Amer. Inst. Aeronaut. Astronaut.*, 2006.

[9] E. Chang, L. Y. Matloff, A. K. Stowers, and D. Lentink, "Soft biohybrid morphing wings with feathers underactuated by wrist and finger motion," *Sci. Robot.*, vol. 5, no. 38, 2020, Art. no. eaay1246.

[10] D. D. Chin, L. Y. Matloff, A. K. Stowers, E. R. Tucci, and D. Lentink, "Inspiration for wing design: How forelimb specialization enables active flight in modern vertebrates," *J. Roy. Soc. Interface*, vol. 14, no. 131, 2017, Art. no. 20170240.

[11] S. Tang and V. Kumar, "Autonomous flight," *Annu. Rev. Control, Robot., Auton. Syst.*, vol. 1, pp. 29–52, 2018.

[12] E. Farrell Helbling and R. J. Wood, "A review of propulsion, power, and control architectures for insect-scale flapping-wing vehicles," *Appl. Mech. Rev.*, vol. 70, no. 1, 2018, Art. no. 010801.

[13] M. Di Luca, S. Mintchev, Y. Su, E. Shaw, and K. Breuer, "A bioinspired separated flow wing provides turbulence resilience and aerodynamic efficiency for miniature drones," *Sci. Robot.*, vol. 5, no. 38, 2020, Art. no. eaay8533.

[14] M. Karásek, F. T. Muijres, C. De Wagter, B. D. Remes, and G. C. de Croon, "A tailless aerial robotic flapper reveals that flies use torque coupling in rapid banked turns," *Science*, vol. 361, no. 6407, pp. 1089–1094, 2018.

[15] L. J. Roberts, H. A. Bruck, and S. Gupta, "Modeling of dive maneuvers for executing autonomous dives with a flapping wing air vehicle," *J. Mechanisms Robot.*, vol. 9, no. 6, 2017, Art. no. 061010.

[16] A. E. Holness, H. Solheim, H. A. Bruck, and S. K. Gupta, "A design framework for realizing multifunctional wings for flapping wing air vehicles using solar cells," *Int. J. Micro Air Veh.*, vol. 11, p. 19, 2019, doi: 10.1177/1756829319836279.

[17] R. Madangopal, Z. A. Khan, and S. K. Agrawal, "Biologically inspired design of small flapping wing air vehicles using four-bar mechanisms and quasi-steady aerodynamics," *J. Mech. Des.*, vol. 127, no. 4, pp. 809–816, 2005.

[18] W. Yang, L. Wang, and B. Song, "Dove: A biomimetic flapping-wing micro air vehicle," *Int. J. Micro Air Veh.*, vol. 10, no. 1, pp. 70–84, 2018.

[19] S. P. Sane and M. H. Dickinson, "The control of flight force by a flapping wing: Lift and drag production," *J. Exp. Biol.*, vol. 204, no. 15, pp. 2607–2626, 2001.

[20] W. Send, M. Fischer, K. Jebens, R. Mugrauer, A. Nagarathinam, and F. Scharstein, "Artificial hinged-wing bird with active torsion and partially linear kinematics," in *Proc. 28th Congr. Int. Council Aeronautical Sci.*, 2012, pp. 1148–1157.

[21] A. Ramezani, X. Shi, S. J. Chung, and S. Hutchinson, "Bat Bot (B2), a biologically inspired flying machine, " in *Proc. Int. Conf. Robot. Aut.*, 2016, pp. 3219–3226.

[22] J. Hoff, A. Ramezani, S. J. Chung, and S. Hutchinson, "Synergistic design of a bio-inspired micro aerial vehicle with articulated wings," in *Proc. Robot.: Sci. Syst.*, 2016, p. 9, doi: 10.15607/RSS.2016.XII.009.

[23] J. Hoff, A. Ramezani, S. J. Chung, and S. Hutchinson, "Optimizing the structure and movement of a robotic bat with biological kinematic synergies," *Int. J. Robot. Res.*, vol. 37, no. 10, pp. 1233–1252, 2018.

[24] J. Hoff, A. Ramezani, S. J. Chung, and S. Hutchinson, "Reducing versatile bat wing conformations to a 1-machine," in *Proc. Conf. Biomimetic Biohybrid Syst.*, 2017, pp. 181–192.

[25] A. Ramezani, S. U. Ahmed, J. Hoff, S. J. Chung, and S. Hutchinson, "Describing robotic bat flight with stable periodic orbits," in *Proc. Conf. Biomimetic Biohybrid Syst.*, 2017, pp. 394–405.

[26] A. Ramezani, X. Shi, S. J. Chung, and S. Hutchinson, "Lagrangian modeling and flight control of articulated-winged bat robot," in *Proc. Int. Conf. Intell. Robots Syst.*, 2015, pp. 2867–2874.

[27] A. Ramezani, X. Shi, S. J. Chung, and S. A. Hutchinson, "Modeling and nonlinear flight controller synthesis of a bat-inspired micro aerial vehicle," in *Proc. Guid., Navigation, Control Conf.*, 2016, Art. no. 1376, doi: 10.2514/6.2016-1376.

[28] J. Hoff, U. Syed, A. Ramezani, and S. Hutchinson, "Trajectory planning for a bat-like flapping wing robot," in *Proc. Int. Conf. Intell. Robots Syst.*, 2019, pp. 6800–6805.

[29] U. A. Syed, A. Ramezani, S. J. Chung, and S. Hutchinson, "From rousettus aegyptiacus (bat) landing to robotic landing: Regulation of CG-CP distance using a nonlinear closed-loop feedback," in *Proc. Int. Conf. Robot. Autom.*, 2017, pp. 3560–3567.

[30] J. W. Bahlman, S. M. Swartz, and K. S. Breuer, "Design and characterization of a multi-articulated robotic bat wing," *Bioinspiration Biomimetics*, vol. 8, no. 1, 2013, Art. no. 016009.

[31] J. Colorado, A. Barrientos, C. Rossi, and K. S. Breuer, "Biomechanics of smart wings in a bat robot: Morphing wings using SMA actuators," *Bioinspiration Biomimetics*, vol. 7, no. 3, 2012, Art. no. 036006.

[32] H. Hauser, A. J. Ijspeert, R. M. Füchslin, R. Pfeifer, and W. Maass, "The role of feedback in morphological computation with compliant bodies," *Biol. Cybern.*, vol. 106, no. 10, pp. 595–613, 2012.

[33] B. P. Trease, Y.-M. Moon, and S. Kota, "Design of large-displacement compliant joints," *Trans. ASME*, vol. 127, pp. 788–798, 2005.

[34] "Digital materials data sheet," 2017. [Online]. Available: https://www.stratasys.com/-/media/files/material-spec-sheets/mss_pj_dig italmaterialsdatasheet_0617a.pdf, Accessed on: May 2020.

[35] U. M. Norberg, "Functional osteology and myology of the wing of the dog-faced bat rousettus aegyptiacus (E. Geoffroy)(mammalia, Chiroptera)," *Zeitschrift Für Morphologie der Tiere*, vol. 73, no. 1, pp. 1–44, 1972.

[36] D. E. Vogtmann, S. K. Gupta, and S. Bergbreiter, "Characterization and modeling of elastomeric joints in miniature compliant mechanisms," *J. Mechanisms Robot.*, vol. 5, no. 4, 2013, Art. no. 041017.

[37] M. Shahzad, A. Kamran, M. Z. Siddiqui, and M. Farhan, "Mechanical characterization and FE modelling of a hyperelastic material," *Mater. Res.*, vol. 18, no. 5, pp. 918–924, 2015.

[38] N. A. Meisel, A. M. Elliott, and C. B. Williams, "A procedure for creating actuated joints via embedding shape memory alloys in polyjet 3D printing," *J. Intell. Mater. Syst. Struct.*, vol. 26, no. 12, pp. 1498–1512, 2015.